Charge-Density Waves in Metallic, Layered, Transition-Metal Dichalcogenides

J. A. Wilson, F. J. Di Salvo, and S. Mahajan
Bell Laboratories, Murray Hill, New Jersey 07974
(Received 4 December 1973)

The previously termed "anomalous" properties of the various polytypes of d^1 TaS_2, $TaSe_2$, etc. are attributed to charge-density waves, their periodic structure distortions, and the superlattices they induce.

The physical properties of the layered transition-metal dichalcogenides, particularly the d^1 metals of group VB, have been the subject of a number of studies.[1] Most of their previously anomalous behavior we now find derives from their unique Fermi surfaces supporting charge-density-wave (CDW) formation. This is the first report of CDW's in other than one-dimensional materials.

Since the metal atom in these layer compounds may be found in either octahedral or trigonal prismatic coordination, and since the layers can be stacked in a variety of ways, a large number of polytypes are found, particularly for TaS_2, $TaSe_2$, and $NbSe_2$. The "anomalous" behavior in resistivity ρ and magnetic susceptibility χ for $1T$-$TaSe_2$ (octahedral coordination) and for $2H$-$TaSe_2$ (trigonal prismatic coordination) can be seen in Figs. 1 and 2. Although these d^1 materials prove to be metallic, one notes that $\rho(300°K)$ for $1T$-$TaSe_2$ is more than an order of magnitude higher than for $2H$-$TaSe_2$; further, $\chi(300°K)$ for $1T$-$TaSe_2$ is actually negative, in contrast to the paramagnetism of $2H$-$TaSe_2$. Clearly of importance, from these and many other measurements, are the *intra*polytypic transitions: here, in $1T$-$TaSe_2$ a first-order one at $T_d = 473°K$, and in $2H$-$TaSe_2$ a second-order one at $T_d = 117°K$. Thermal studies show that ΔH at T_d for $1T$-$TaSe_2$ is ~300 cal/mole, while the integrated heat of transition for $2H$-$TaSe_2$ is only ~1 cal/mole.[1] Other polytypes of $TaSe_2$, and similar ones for $NbSe_2$ and TaS_2, show basically similar behavior, though the details, especially as reflected in ρ, are often more complex.

Electron diffraction at 200 kV, with the beam at normal incidence to the layers, yields to well above T_d a marked diffuse scattering pattern, but below T_d we see just the sharp spotting of a superlattice. Plates for $1T$-$TaSe_2$ are shown in Fig. 3. From previous x-ray studies one would have expected only the spots separated by the basic reciprocal lattice vector $\vec{a}_0^*$. It is clear that both above and below T_d additional spots occur.

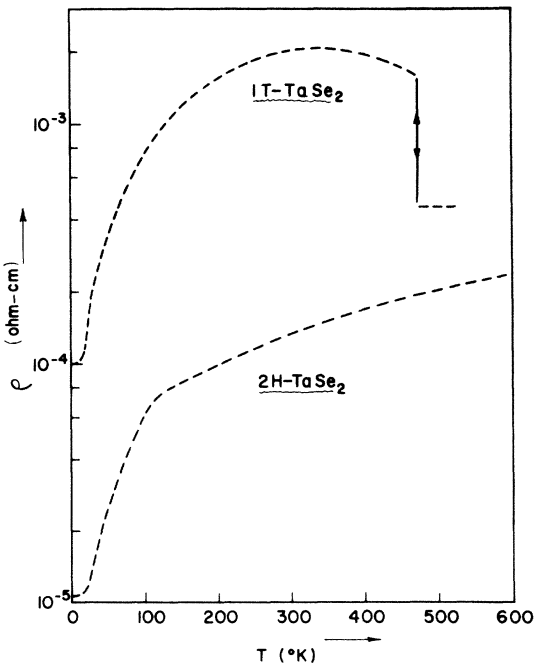

FIG. 1. Resistivity of $1T$-$TaSe_2$ and $2H$-$TaSe_2$ parallel to the layers.

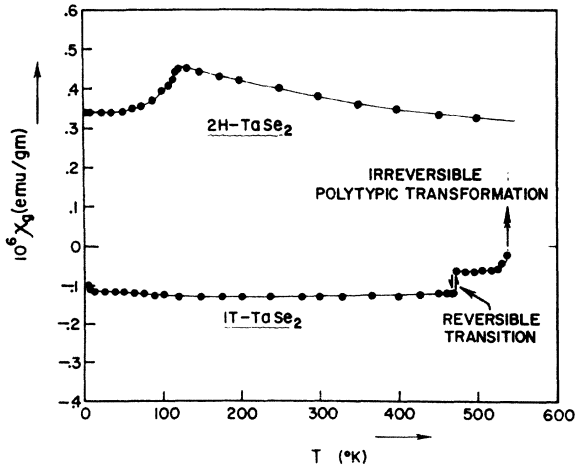

FIG. 2. Magnetic susceptibility of random powders of $1T$-$TaSe_2$ and $2H$-$TaSe_2$.

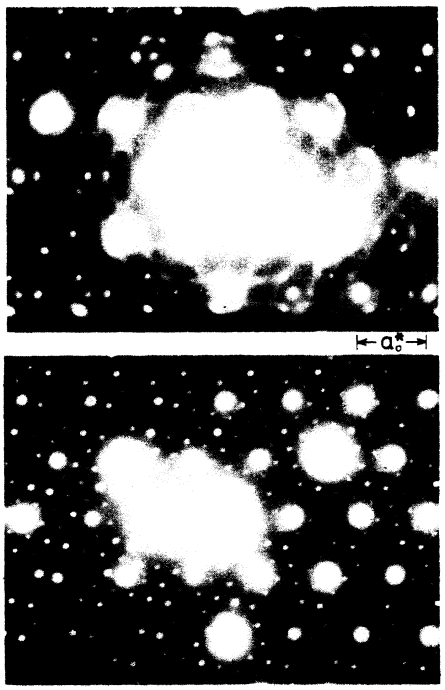

FIG. 3. $1T$-$TaSe_2$ electron diffraction patterns (basal plane) (a) just above T_d and (b) just below T_d.

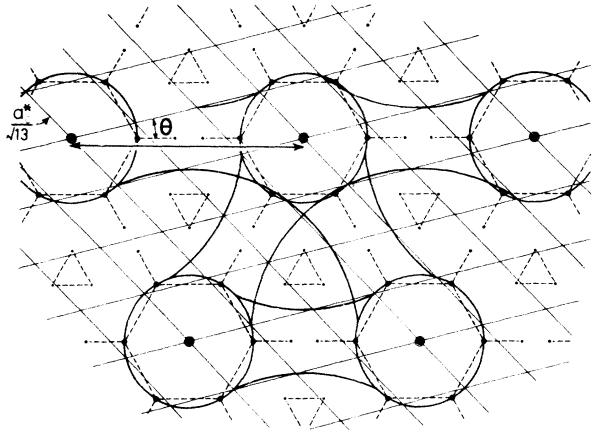

FIG. 4. Geometric relationship between the electron diffraction pattern above T_d to that below for $1T$-$TaSe_2$. (All straight lines serve merely to draw attention to the pattern periodicity.) In the low-temperature superlattice condition spots appear at all intersections of the rhombohedral network. $\theta = 13°54'$. Double-headed arrow, a_0^*.

For $1T$-$TaSe_2$ we observe that at T_d a rotated superlattice (i.e., $\vec{a}$ not parallel to $\vec{a}_0$) of side $a = \sqrt{13}\,a_0$ suddenly is adopted.[2] In reciprocal space we see the supercell vector $\vec{a}^*$ to be of the same magnitude as the radius of the first ring of diffuse scattering, namely $a_0^*/3.6$. Above T_d,[3] besides the rings of diffuse scattering, extra fairly sharp spots are also evident. These satellite spots are all separated from their parent Bragg peaks by vectors based on the unit of $a_0^*/3.6$. The detailed geometric relationship between the diffraction patterns shown by $1T$-$TaSe_2$ above and below T_d is given in Fig. 4. The sudden adoption of the $\sqrt{13}\,a_0$ superlattice at T_d in $1T$-$TaSe_2$ is of quite different character from what happens at the second-order transition in $2H$-$TaSe_2$. There a gradual buildup of diffuse scattering around $\vec{a}^* = \vec{a}_0^*/3$ gives place below 117°K to sharp spots forming at precisely those points. However, all the intrapolytypic changes reflect some drive towards superlattice formation, a drive which we shall show derives from the Fermi surfaces and the CDW's they support.

The effect of Ti substitution for Ta is to stabilize the $1T$ polytype. Suppression then of the $\sqrt{13}\,a_0$ superlattice is finally completed at about 15% Ti, but anomalous behavior in ρ and χ persists up to about 80% Ti. Strong diffuse electron scattering still holds through this nonsuperlattice regime, though it falls off in intensity at the highest Ti contents. (The satellite spots mentioned earlier disappear rather quickly.) We plot in Fig. 5 the radii found for the smaller "circle" of diffuse scattering versus x through the series $Ta_xTi_{1-x}S_2$. The diffuse scattering looks almost identical in the $Ta_xTi_{1-x}Se_2$ series, but we have more data for the sulphides.

The observation that the diffuse scattering radius depends upon the Ti concentration in the above manner indicates (as expanded upon below)

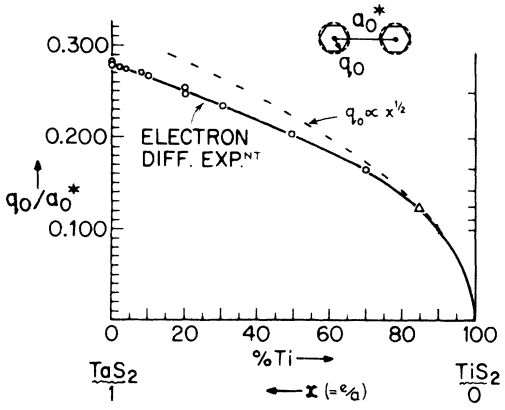

FIG. 5. Observed decrease in magnitude of the diffuse scattering vector through the alloy sequence $1T$-$(Ta_xTi_{1-x})S_2$. $(1/\sqrt{13} = 0.2783.)$

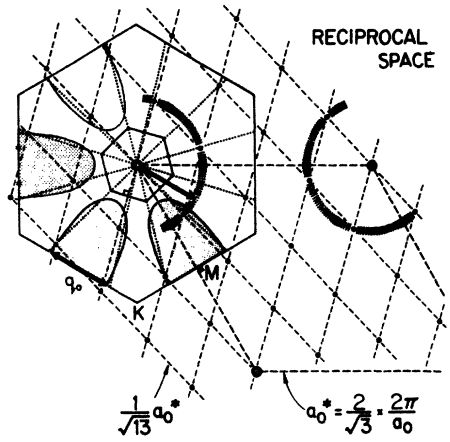

FIG. 6. 2D Fermi surface of $1T$-TaS_2 in plan, showing the spanning vector q_0, the smaller radius of diffuse scattering, the low-temperature superlattice, and the Brillouin zones for above and below T_d. [The larger circle of diffuse scattering (see Figs. 3 and 4) is from an umklapp process.]

that the scattering is related to the Fermi-surface geometry. The Fermi surface for $1T$-$TaSe_2$, as generated from the calculation of Mattheiss,[4] is included in Fig. 6 in basal projection. The surface is almost independent of k_z, reflecting strongly the layered nature of the compound. The vector $\vec{q}_0$ spanning the Fermi surface at the hexagonal Brillouin zone (BZ) faces is seen to equal the radius of the smaller circle of diffuse scattering (hatched area in Fig. 6). As one reduces x (the number of electrons per atom) the Fermi surface then shrinks back steadily upon the vertical ML axes, in the manner anticipated from the calculations for $1T$-$TaSe_2$ and $TiSe_2$, presuming a rigid-band behavior for these virtually isometric $5d^1/3d^0$ alloys.

The Fermi surface for $2H$-$TaSe_2$ is more complex because there are now two metal atoms per unit cell. This leads to a two-sheeted Fermi surface. However, we believe that the critical $\vec{q}_0$ is again at the BZ face, where we find a length in close accord with the $q_0 = a_0^*/3$ of experiment.

Theoretical work[3] suggests that the compounds are likely to be susceptible to Fermi-surface–driven instabilities, like a strong Kohn anomaly, a CDW, or a spin-density wave (SDW). Large, essentially parallel sections of Fermi surface, spanned by wave vector $\vec{q}_0$, lead in the real space potential to a strong oscillatory component of wavelength $1/q_0$.[5,6] Ultimately the situation can lead to a divergence in the generalized susceptibility $\epsilon(\vec{q})$ at $\vec{q}_0$.[7] With a CDW, prior to any lock-in to the lattice, diffuse scattering and lack of definition in the diffraction pattern may arise because the domains over which the CDW holds phase or selected orientation are small. Further, the wavelength is not uniquely defined for $T \neq 0$. Also, long-lived fluctuations to the superlattice condition, or the soft-mode scattering of a deepening Kohn anomaly, may occur. Whether it should be a CDW or a SDW (as in Cr) that finally might form will depend upon the relative magnitude of the electron-electron and electron-phonon interactions used to renormalize the bare susceptibility $\epsilon^0(\vec{q})$. The appropriate parameters here will, we believe, satisfy criteria as recently formulated by Chan and Heine[8] for there to be a CDW in $4d^1/5d^1$, $NbSe_2$, etc., with possibly a SDW in the $3d$ alloy system $V_xTi_{1-x}S_2$.

Any CDW must introduce a periodic structural distortion (PSD) of the same period, one that is, in general, incommensurate with the lattice. As the temperature is decreased, the increasing amplitude of this PSD will favor lock-in to some suitably commensurate period, so that strain energies may be minimized. Adding to the above drive, particularly for these tight-binding solids, is the fact that the charge maxima in the CDW will center then upon cation sites. This is what is achieved in $1T$-$TaSe_2$ with the rotational lock-in; the initially dominant periodicity of roughly $3.6a_0$, fed in parallel to $\vec{a}_0$, adjusts to $\sqrt{13}\,a_0$ (i.e., $3.606a_0$) rotated away by $\tan^{-1}(\sqrt{3}/7)$ (i.e., 13°54′) from the "input" direction. (Domains of positive and negative rotation have been observed.) The process can secure a large decrease in Fermi-surface area within the reduced zone of the superlattice. For $1T$-$TaSe_2$ the marked discontinuity in ρ at T_d indicates a decrease there of about 90%. The infrared metallic reflectivity is made to become even more "anomalous" than it was above T_d under the incommensurate CDW (Wilson, Ref. 1). In general any appreciable cation disorder, even as in $5d^1/4d^1$ $1T$-$(Ta_{0.6}Nb_{0.4})S_2$, is found to withold lock-in to a superlattice condition. Carrier scattering, even within a disturbed superlattice, can become so severe that, on cooling, ρ continuously *in*creases.

In our various superlattices, the associated atomic displacements amount only to about 0.05 to 0.10 Å. By contrast, for $2H$-$NbSe_2$ ($T_d \sim 35$°K) the earlier NMR results[9] indicated that the Nb atom sites must pick up by 4°K site charge inequivalencies of as much as 5%.

In conclusion, we have shown not only the source of anomalous behavior in these layer com-

pounds, but have thereby provided the first observation of CDW's in other than one-dimensional (1D) metals. Since their electron concentration can be varied by doping, and since different band structures are provided by the different polytypes, these layer systems offer greater latitude for study than do the 1D metals like $K_2Pt(CN)_4 \cdot Br_{0.30} \cdot 3H_2O$.[10] The 1D metals have point Fermi "surfaces" and just the one spanning vector. We have now found a CDW occurring in a case where there are several possible perhaps competing spanning vectors.

The existence of a CDW/PSD in $2H$-$TaSe_2$, etc. brings property changes that appear very similar to those occurring in $A15$'s like Nb_3Sn, at and below the Batterman-Barrett transition. For both groups of materials there results an intriguing interplay with the superconducting properties.

A much fuller account of the electron diffraction studies on many of these layered compounds has been submitted elsewhere. Studies of the transport, magnetic, and superconducting properties, and of the effects of intercalation are also to be published.

[1]F. J. Di Salvo, B. G. Bagley, J. M. Voorhoeve, and J. V. Waszczak, J. Phys. Chem. Solid 34, 1357 (1973); F. J. Di Salvo, R. G. Maines, J. V. Waszczak, and R. E. Schwall, to be published. J. A. Wilson and A. D. Yoffe, Advan. Phys. 18, 193 (1969); A. D. Yoffe, in *Festkörperprobleme*, edited by H.-J. Queisser (Pergamon, New York, 1973), Vol. 13, p. 1; J. A. Wilson, to be published.

[2]Throughout we label this supercell "$\sqrt{13}\,a_0$," as defined in a strictly hexagonal $\Delta V = 0$ supercell by the vector [310]. Actually $\Delta V \approx -0.38\%$, and the supercell is triclinic pseudohexagonal.

[3]A. W. Overhauser, Phys. Rev. 167, 691 (1968).

[4]L. F. Mattheiss, Phys. Rev. Lett. 30, 784 (1973), and Phys. Rev. B 8, 3719 (1973).

[5]L. M. Roth, H. J. Zeiger, and T. A. Kaplan, Phys. Rev. 149, 519 (1966).

[6]S. C. Moss, Phys. Rev. Lett. 22, 1108 (1969).

[7]C. Herring, in *Magnetism*, edited by G. T. Rado and H. Suhl (Academic, New York, 1966), Vol. IV.

[8]S.-K. Chan and V. Heine, J. Phys. F: Metal Phys. 3, 795 (1973).

[9]E. Ehrenfreund, A. C. Gossard, F. R. Gamble, and T. H. Geballe, J. Appl. Phys. 42, 1491 (1971).

[10]B. Renker, H. Rietschel, L. Pintschovius, W. Gläser, P. Brüesel, D. Kuse, and M. J. Rice, Phys. Rev. Lett. 30, 1144 (1973).

Spontaneous Interconfiguration Fluctuations in the Tm Monochalcogenides

M. Campagna, E. Bucher, G. K. Wertheim, D. N. E. Buchanan, and L. D. Longinotti
Bell Laboratories, Murray Hill, New Jersey 07974
(Received 19 February 1974)

Spontaneous interconfiguration fluctuations have been detected in TmTe and TmSe by x-ray photoemission. The resulting instantaneous picture of the Tm ions fluctuating between the divalent and trivalent state within the same environment allows a direct measurement of the magnitude of the Coulomb correlation energy, U_{eff}. Spontaneous interconfiguration fluctuations are shown also to affect the binding energies of core levels within the same rare-earth ion, resulting in a chemical shift of 3.5 ± 0.1 eV for the Tm($5p$) core levels.

Temporal valence fluctuations between two distinct configurations of a rare-earth (RE) $4f$ shell have been recently interpreted to be the source of the demagnetization of RE ions in dilute and concentrated alloy systems.[1,2] According to this concept, nonmagnetic behavior of a strongly localized $4f$ shell is related to a nonintegral, time-averaged occupation of that shell. Generally speaking, the phenomenon of spontaneous interconfiguration fluctuations (ICF), introduced by Hirst,[1] and based on a modification of the Friedel-Anderson model of local-moment formation,[3] seems successfully to connect the experimental fact of nonmagnetic behavior in the collapsed phase of, for example, SmS or SmB_6 with spontaneous valence fluctuations in the $4f$ shell.

The purpose of this Letter is to present direct experimental evidence for the existence of such fluctuations, based on high-resolution x-ray photoemission spectroscopy (XPS). Since photoexcitation takes place in a time short compared to that assumed for the fluctuations (up to 10^6–10^7 times shorter) it should be possible to observe the instantaneous picture of the ions in the two valence states. The same measurement then also allows a direct measurement of the intra-

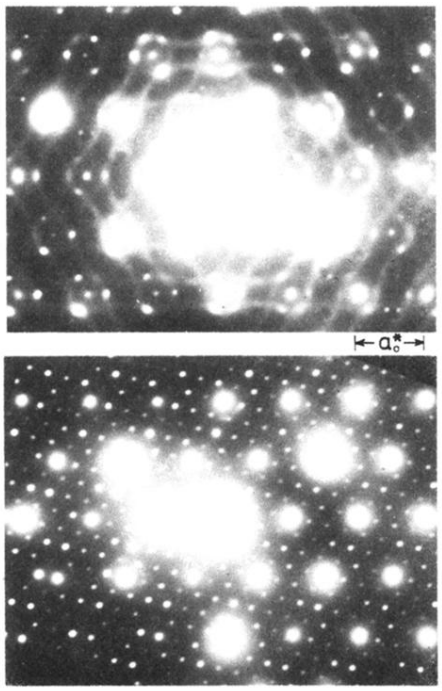

FIG. 3. $1T$-$TaSe_2$ electron diffraction patterns (basal plane) (a) just above T_d and (b) just below T_d.

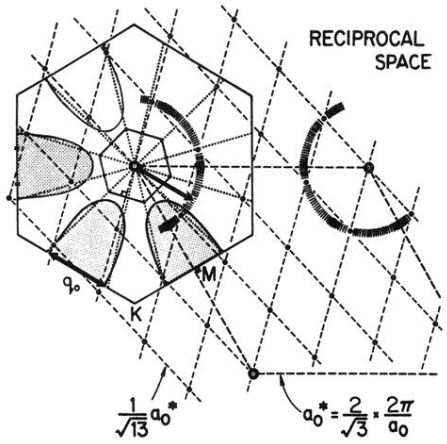

FIG. 6. 2D Fermi surface of $1T$-TaS_2 in plan, showing the spanning vector q_0, the smaller radius of diffuse scattering, the low-temperature superlattice, and the Brillouin zones for above and below T_d. [The larger circle of diffuse scattering (see Figs. 3 and 4) is from an umklapp process.]